The Cryosphere Discussions

Modelling borehole temperatures in Southern Norway – insights into permafrost dynamics during the 20th and 21st century

T. Hipp, B. Etzelmüller, H. Farbrot, T. V. Schuler, and S. Westermann

Department of Geosciences, University of Oslo, Oslo, Norway

Correspondence to: T. Hipp (tobias.hipp@geo.uio.no)

Title Page

Abstract	Introduction
Conclusions	References
Tables	Figures

Back | Close

Full Screen / Esc

Printer-friendly Version

Interactive Discussion

Modelling borehole temperatures in Southern Norway

T. Hipp et al.

Abstract

A transient heat flow model was used to simulate both past and future ground temperatures of mountain permafrost and associated active layer thickness in Southern Norway. The model was forced by reconstructed air temperature starting from 1860, approximately coinciding with the Little Ice Age in the region. The impact of climate warming on mountain permafrost until 2100 is assessed by using downscaled air temperatures from a multi-model ensemble for the A1B scenario. For 13 borehole locations, records over three consecutive years of ground temperatures, air temperatures and snow cover data are available for model calibration and validation. The boreholes are located at different elevations and in substrates with different thermal properties. With an increase of air temperature of $\sim$ +1.5 °C over 1860–2010 and an additional warming of +2.8 °C until 2100, we simulate the evolution of ground temperatures for the borehole locations. According to model results, the active-layer thickness has increased since 1860 by 0.5–5 m and > 10 m for the sites Juvvasshøe and Tron, respectively. The simulations also suggest that at an elevation of about 1900 m a.s.l. permafrost will degrade until the end of this century with a probability of 55–75 % given the chosen A1B scenario.

1 Background and objectives

Permafrost in general and mountain permafrost in particular experience increasing interest due to their sensitivity to climate variation and importance for geomorphologic and geotechnical processes (Harris et al., 2009), such as slope stability and natural hazards (Gude and Barsch, 2005; Huggel et al., 2010; Gruber et al., 2004a; Fischer et al., 2006; Haeberli, 1992). Quantitative assessments of ground thermal regimes are of importance for understanding surface and sub-surface processes in mountain environments. Thus, there is a need to address the response of ground temperatures (GT) to climate forcing, especially the modulation of the response of GTs to the effect

of snow cover and different types of surficial material and bedrock.

In Scandinavia and especially in Northern Norway, Iceland and Svalbard, multiple shallow boreholes have been drilled to continuously monitor ground thermal regimes and the relation between atmosphere and ground in terms of energy exchange since 1999 (Christiansen et al., 2010; Etzelmüller et al., 2007; Farbrot et al., 2007; Isaksen et al., 2000, 2003). In 2008 12 new boreholes have been established at three different mountain areas in Southern Norway. This monitoring network addresses environmental gradients in Southern Norway related to elevation and continentality (Farbrot et al., 2011), and provides the basis for calibrating and validating transient heat flow models.

One-dimensional heat flow models have been applied in various permafrost studies to assess the response of permafrost to climate change, such as in Canada (Burn and Zhang, 2009; Zhang et al., 2006, 2008), the Russian arctic (Malevsky-Malevich et al., 2001; Romanovsky et al., 2007; Sazonova et al., 2004), Svalbard (Etzelmüller et al., 2011, this issue) and Alaska (Biesinger et al., 2007; Osterkamp and Romanovsky, 1999) and in even more complex mountain regions such as the European Alps (Engelhardt et al., 2010; Gruber and Hoelzle, 2008; Gruber et al., 2004b; Hoelzle et al., 2001; Luetschg et al., 2008; Noetzli and Gruber, 2009; Noetzli et al., 2007; Scherler et al., 2010; Stocker-Mittaz et al., 2002).

The objective of this study is to assess the ground thermal response ~~of permafrost~~ to historical and future air temperature (T_{AIR}) variation in different environmental settings in terms of elevation, snow and sediment cover for mountain sites in Southern Norway. The study aims for quantifying subsurface warming and changes in active layer thickness (ALT) over a c. 250 yr period from the approx. end of the Little Ice Age (LIA) in the mid 19th century to 2100 in the high-mountain environment of Southern Norway. Over this period, significant warming occurred and is expected to continue. In relation to these changes, we intend to identify the possible zonations of former, present and future permafrost. Finally, we aim to characterise these responses for different environmental settings in terms of bedrock properties, sediment-cover and snow. We suggest that these assessments are fundamental prerequisites for spatially distributed

permafrost modelling in Scandinavia, and for understanding geomorphological process patterns and ultimately landscape development (Berthling and Etzelmüller, 2011).

In this study, we apply a 1-D heat flow model (Etzelmüller et al., 2011; Farbrot et al., 2007) to simulate GTs and ALT for the time period of 1860 until 2100. The model was first calibrated and validated for each of totally 13 sites, where records of GT, GST and T_{AIR} exist. Forcing the calibrated model using reconstructed and projected T_{AIR} series, we assess how sensitive GT and ALT react to warming at the investigated sites, including an assessment of model limitations and related uncertainties of our approach.

2   Setting, instrumentation and climate at the study sites

We use borehole measurements from three locations in Southern Norway in this study (Fig. 1a): Juvvasshøe (61°40′ N, 08°22′ E, 1894 m a.s.l.), Jetta (61°53′ N, 9°17′ E, 1640 m a.s.l.) and Tron (62°10′ N, 10°41′ E, 1560 m a.s.l.). At these sites, ground temperature records are available for 13 boreholes at 2-h intervals covering the period August 2008 to July 2011. At Juvvasshøe, the PACE borehole ground temperature data is available from 1999 (Isaksen et al., 2001, 2007). An overview of the geomorphologic and climatic setting as well as the permafrost conditions at the study sites are given here, while a more detailed description of the sites and the instrumentation is given by Farbrot et al. (2011).

2.1   The borehole sites and instrumentation

Juvvasshøe (1894 m) (Fig. 1b) has a comparatively long history of permafrost research (Isaksen et al., 2001, 2002, 2003; Ødegård et al., 1988, 1992, 1996, 1999) with first ground temperature measurements started by Ødegård et al. (1992) and the later drilling of the 129 m deep PACE borehole (Harris et al., 2001; Isaksen et al., 2001). The surface of the site is characterized by extensive block fields at higher elevations and finer till material at lower elevations (Ødegård et al., 1988). Six boreholes were drilled

Modelling borehole temperatures in Southern Norway

T. Hipp et al.

in addition to the existing PACE borehole along an altitudinal transect from 1894 m a.s.l. (PACE) down to 1307 m a.s.l. (Juv-BH6) (Fig. 1b). The boreholes have different stratigraphies: PACE, Juv-BH1 and Juv-BH3 are located in block fields, Juv-BH4 was drilled in bedrock and Juv-BH6 in a sand- to gravel-rich ground moraine.

At *Jetta* (Fig. 1c) block fields are present down to elevations of 1500 m and 1100 m a.s.l. on the north and south exposition, respectively, with thicknesses ranging from 3 to 10 m (Bø, 1998). Three boreholes were drilled 10 m into bedrock at 1560 m a.s.l. (Jet-BH1), 1450 m a.s.l. (Jet-BH2) and 1218 m a.s.l. (Jet-BH3), respectively.

Tron (Fig. 1d) is located further east in a more continental climate setting. Two boreholes were drilled 10 m into fine-grained morainic material, while the uppermost borehole (Tro-BH1, 1640 m) was drilled 30 m into a block field.

At all boreholes GST, T_{AIR} and snow depth (SD) are recorded. Maxim[©] iButton temperature loggers ($\pm 0.5\,^\circ$C accuracy) at fixed heights above the ground surface (10, 20, 30, 40, 50, 60, 80, 100, 120 cm) were used to extract the snow depth using the daily temperature variance (Lewkowicz, 2008). At PACE and Tron automatic weather stations record several meteorological variables to characterize the surface energy balance.

2.2 Climate and ground thermal conditions at the study sites

The three sites are situated along a continentality gradient from a more maritime influenced climate at Juvvasshøe to a more continental climate setting at Tron (Farbrot et al., 2011). The entire period was divided in three seasons (S1 – September 2008 to August 2009; S2 – September 2009 to August 2010; S3 – September 2010 to July 2011) to analyze the inter-annual variation (Table 1). S3 does not cover a complete season and is therefore not used for the comparison of mean annual air temperatures (MAAT), seasonal variations or *n*-factor calculations.

At Juvvasshøe MAATs during S1 and S2 ranged from $-3.4\,°C$ to $-0.6\,°C$ and $-4.5\,°C$ to $-2.3\,°C$, respectively, resulting in an average altitudinal lapse rate of $0.5\,°C/100\,m$ (Farbrot et al., 2011). At higher elevations snow cover is strongly variable and generally thin ($< 20\,cm$) due to strong redistribution by wind. A thick snow cover, however, is found at lower elevations (70–$140\,cm$) (Table 1). Permafrost is present at BH4 at $1559\,m$ a.s.l. and the lower limit of permafrost along the instrumented slope was c. $1450\,m$ a.s.l. (Farbrot et al., 2011). Permafrost thickness at the PACE borehole was estimated to be approximately $380\,m$ (Isaksen et al., 2001). During the study period, observed ALT varied between 1.6 (Juv-BH1) and $8.6\,m$ (Juv-BH4) and seasonal frost depths between $0.5\,m$ and $> 6\,m$ (not shown). The mean annual ground temperature at $10\,m$ depth ($MAGT_{10}$) ranges from $-2.4\,°C$ to $-0.5\,°C$ within permafrost and reaches up to $+1.7\,°C$ (Juv-BH6) in non-permafrost areas.

At Tron, MAAT during S1 and S2 ranged from $-3.6\,°C$ to $-0.9\,°C$ and $-4.5\,°C$ to $-2.3\,°C$, respectively. Tro-BH1 and Tro-BH2 show thick and long-lasting snow cover during both seasons ($> 90\,cm$). Permafrost was found at the uppermost borehole with GTs only slightly below $0\,°C$ down to a depth of $30\,m$. Despite lower MAAT and MAGST in S2, the ALT at Tron-BH1 slightly increased from $10.7\,m$ to $11.1\,m$ (Fig. 3c). Along the north slope of Tron, comparatively low MAGST of $-0.4\,°C$ to $-0.7\,°C$ were recorded by miniature temperature loggers down to $1450\,m$ a.s.l., indicating the possible presence of permafrost (Farbrot et al., 2011). Seasonal frost dominates at the lower boreholes with freezing depths of c. $1.5\,m$ to $4\,m$. Similarly an increase of freezing depths was observed during S2 and S3 (Fig. 3d).

At Jetta, MAATs between $-2.2\,°C$ to $-0.2\,°C$ and $-3.7\,°C$ to $-1.6\,°C$ were measured during S1 and S2, respectively. A long-lasting, thick snow cover ($> 140\,cm$) is recorded at the uppermost two boreholes, while Jet-BH3 had no significant snow cover due to strong wind drift. Therefore, despite the lower elevation, the GST recorded at Jet-BH3 is lower than at Jet-BH2 (Table 1). The uppermost ($1560\,m$ a.s.l.) borehole record shows permafrost with a $MAGT_{10}$ of $-0.8\,°C$ and an ALT decreasing from c. $8.0\,m$ to c. $6.9\,m$ during the observation period (Table 3). While at Jet-BH2 the depth of seasonal

frost remains at c. 6.5 m due to a constant snow cover, an increase from c. 6 m to c. 9 m depth was observed at Jet-BH3 (Fig. 3f).

2.3 Seasonal variations

The air temperature records for different sites and seasons display the influence of continentality as well as a strong inter-annual variation. To better analyse these differences, we calculated anomalies of mean monthly air temperatures (MMAT) for all three sites ~~and~~ for 2008–2011 with respect to the reference period 1961–1990 (Fig. 2, see Sect. 3.2 for details). Due to the lower elevation, Jetta shows higher summer and winter temperatures. However, although Tron is about 250 m lower than Juvvasshøe, T_{AIR} is similar or even lower (Fig. 2a). Using altitudinal lapse rates derived from observations (Farbrot et al., 2011), MAAT at 1640 m a.s.l. is −2.3, −2.2 and −3.8 °C at Juvvasshøe, Jetta and Tron, respectively. Two different seasonal patterns have been observed (Fig. 2b). Compared to the normal period S1 was warmer by 1.0 °C to 1.7 °C. The MAAT of S2, however, was −0.5 °C lower at Juvvasshøe and 0.3 °C to 0.4 °C higher at the other sites. The MAAT during S2 was on average by 1.4 °C to 1.1 °C lower than during S1. At PACE the winter 2008–2009 did not show any strong deviation from the period 1961–1990, but positive deviations of up to +5 °C were recorded during spring and summer. The winter 2009/2010 was much colder than the normal period, with negative deviations of up to −4.5 °C during December to February (Fig. 2b).

The borehole temperatures show different susceptibilities to inter-annual variability depending on the strength of coupling between GST and T_{AIR} (Fig. 4). Boreholes having a close atmosphere-ground coupling show much lower GSTs and GTs in S2. The GSTs of S2 at Juv-BH3 and the bedrock site Juv-BH4 were by 0.6 °C and 2.1 °C lower, respectively, than during S1 (Table 1). While Jet-BH2 shows a constant MAGST of +0.9 °C during both seasons due to extensive snow cover, strong variations at Jet-BH3 with +0.5 °C during S1 and −1.0 °C during S2 (Table 1) demonstrate closer coupling between atmosphere and ground surface (Fig. 4).

Title Page

Abstract | Introduction

Conclusions | References

Tables | Figures

◄◄ | ►►

◄ | ►

Back | Close

Full Screen / Esc

Printer-friendly Version

Interactive Discussion

3 Methods

3.1 1-D numerical heat flux model

For this study we used a one-dimensional transient heat flow model, which was previously applied in similar studies (Farbrot et al., 2007; Etzelmüller et al., 2011). Assuming heat conduction as the only process of energy transfer the model is solving the heat conduction equation (Williams and Smith, 1989)

$$\rho c_{eff} \frac{\partial T}{\partial t} = \frac{\partial}{\partial z}\left(k \frac{\partial T}{\partial z}\right) \tag{1}$$

describing the evolution of the ground temperature T over time t and depth z, where specific heat capacity c_{eff}, thermal conductivity k and density ρ are the main thermal properties of the ground. All borehole stratigraphies were implemented in the model at a spatial resolution of $\Delta z = 0.1$ m by assigning ground thermal properties according to the observed stratigraphy (Table 2). The heat conduction equation (1) is then solved using finite differences along the borehole profile to a depth of 150 m. The volumetric water content (VWC) is considered in the model as a constant. The effect of latent heat due to freezing and thawing of the ground is accounted for by using a temperature-dependent effective heat capacity c_{eff}, which is strongly increased in a temperature interval of $\pm 0.1\,°C$ around the freezing temperature of the pore water (Etzelmüller et al., 2011). Any effects related to the advection of heat due to flow of ground water or of air in coarse-grained block fields are not considered in the model formulation.

3.2 Historic and future temperature data

Analyzing available long-term temperature records (starting in the 1860s), Hanssen-Bauer (2005) and (Hanssen-Bauer and Nordli, 1998) identified six temperature regions, each of which characterized by similar long-term variability of air temperature. For each region monthly standardised temperature series ST_m are derived by averaging

the standardized temperature series $ST_{m,i}$ of each individual station i in the region m:

$$ST_m = (1/n) \times \sum_{i=1}^{n} ST_{m,i} \qquad (2)$$

The individual standardized series are presented as anomalies in terms of standard deviations $\sigma_{T_{m,i}}$ relative to the 1961–1990 average $\mu_{T_{m,i}}$ (Hanssen-Bauer, 2005):

$$ST_{m,i} = (T_{m,i} - \mu_{T_{m,i}})/\sigma_{T_{m,i}} \qquad (3)$$

where $T_{m,i}$ is the observed temperature series at station i in region m.

For the entire mainland Norway MDATs are available as 1-km-resolution maps ($MDAT_{grid}$) for the period 1 September 1957 until present (provided by the Norwegian Meteorological Institute – met.no, available at http://senorge.no, from hereon referred to as *seNorge* dataset). These grids are interpolated (*kriging*) from recorded temperatures at synoptic weather stations (Mohr, 2009). Daily air temperatures from 1957 to 2008 were generated for the boreholes PACE, Jet-LB1 and Tro-BH1 using linear regressions between measured temperatures and those extracted from *seNorge* for the corresponding location. This procedure worked well for PACE with $r^2 = 0.8$ and a RMSE of 3.1 °C. For Jet-LB1 and Tro-BH1, however, the relation between observed air temperature and the corresponding *seNorge* value is non-linear, displaying a sharp bend at low temperatures. This characteristic is associated with the frequent occurrence of temperature inversions during winter (Farbrot et al., 2011), which are not captured by the *seNorge* dataset. To cope with this problem two separate linear regressions were performed for each site, one above and one below a threshold temperature (-10 °C and -5 °C for Tro-BH1 and Jet-BH1, respectively).

For the normal period 1961–1990 mean monthly values ($MAT_{i,1961-1990}$) and monthly standard deviations ($\sigma_{1961-1990}$) were calculated from these daily air temperatures. ST_m was used to construct a time series of monthly air temperatures at the station i (MAT_i) from the early 1860ies until today at the station i by (Hanssen-Bauer, 2005):

$$MAT_i = MAT_{1961-1990} + ST_m \times \sigma_{1961-1990} \qquad (4)$$

Modelling borehole temperatures in Southern Norway

T. Hipp et al.

Title Page

Abstract | Introduction

Conclusions | References

Tables | Figures

◄ | ►I

◄ | ►

Back | Close

Full Screen / Esc

Printer-friendly Version

Interactive Discussion

The observed temperature lapse rates during 2008–2010 of 0.5, 0.6 and 0.8 °C/100 m at Juvvasshøe, Jetta and Tron, respectively (Farbrot et al., 2011), were used to transfer the so-constructed MAT_i time series locally to the other borehole locations. The historic air temperature series used as input data for the modelling therefore consists of monthly values until 2008 and measured daily values for 2008–2011.

Concerning the future air temperature series for the climate change model runs, the rather moderate A1B emmission scenario was chosen. The A1B scenario assumes balanced use of all energy sources with an increase in renewable energy sources, therefore assuming a decrease of CO_2 emissions by the mid of the 21st century (IPCC, 2007). The likely range of the global mean temperature change from 1990 to 2100 of the A1B scenario is between +1.7 °C and +4.4 °C, with a best estimate of +2.8 °C (IPCC, 2007). Temperatures from an ensemble of > 30 different GCMs were empirically-statistically downscaled to the weather station *Fokstugu* (Benestad, 2011, 2005), which is located between the Jetta and Tron sites, and used to drive the ground heat flux model. The measured daily air temperatures at each borehole were correlated to Fokstugu yielding r^2-values of > 0.9. This allowed the construction of air temperature scenarios for each individual borehole from 2010 until 2100 by correcting for a constant bias, specific for each site (Fig. 8a).

3.3 Model initialization and boundary conditions

The finite-difference scheme for solving Eq. (1) requires boundary conditions at the upper and lower ends of the domain. Here, we used a geothermal heat flux of $Q_{geo} = 33\,\text{mW m}^{-2}$ (Isaksen et al., 2001) as lower boundary condition and GST as upper boundary condition.

The atmosphere-ground coupling is an important factor for prescribing appropriate upper boundary conditions for the heat flow model. The relation between T_{AIR} and GST varies strongly from borehole to borehole, depending on snow and surface cover (Fig. 4). Historical and future time series of GST were generated from the reconstructed T_{AIR} and downscaled future temperatures, respectively, using n-factors. n-

factors are considered as transfer functions relating T_{AIR} to GST during freezing (n_F) and thawing (n_T) conditions (Smith and Riseborough, 2002; Lunardini, 1978). The n-factors were derived from measured daily GST and T_{AIR} at each borehole by calculating the ratios of annual sums of freezing (FDD) and thawing degree days (TDD) of GST to those of T_{AIR}:

$$n_F = \frac{FDD_S}{FDD_A} \tag{5}$$

$$n_T = \frac{TDD_S}{TDD_A} \tag{6}$$

where indices S and A refer to the temperature at the ground surface and the air, respectively (Riseborough, 2007). FDD and TDD were calculated for the whole year and not based on freezing and thawing seasons at the ground surface, using average daily air temperatures. Sites having a thick snow cover are characterized by a GST > T_{AIR} during large parts of the winter and therefore $n_F < 1$. $n_T > 1$ indicates a higher GST than T_{AIR} during summer, which can be the case at bedrock sites in the absence of vegetation or on south-facing slopes.

The reconstruction of historic permafrost conditions employs monthly air temperatures whereas n-factors were determined from diurnal data. We investigated the possible effect of this inconsistency in temporal resolution on the n-factor values by recalculating n-factors based on monthly data. We found that the values deviate by less than 9 % and therefore, we use the same n-factors throughout our study, regardless of whether they were applied to monthly or daily temperatures. For the long term modelling, mean values of n_F and n_T of S1 and S2 were used (Table 1), assuming representativeness of our observation period. n_F-values range from 0.2 and 0.4 at boreholes with a thick snow cover (Tr-BH1, Tr-BH2, Jet-BH1, Jet-BH2 and Juv-BH6) and from 0.8 to 1.0 where snow cover was moderate (Table 1). n_T-values > 1.2 were obtained for bedrock boreholes without vegetation cover.

The model was initialised in two different ways, one for the calibration and validation procedure and the other one for the historical permafrost modelling. Simulations of S1 and S2 were initialised from observed profiles of GT which were extrapolated to the full depth assuming a linear gradient. Longterm simulations were started from steady-state corresponding to the mean air temperature of the decade 1860–1869. To account for seasonal variations a second degree Fourier curve function,

$$T = a_0 + \sum_{i=1}^{2} a_i \cos(i\omega t) + b_i \sin(i\omega t), \tag{7}$$

is fitted to the observed daily T_{AIR} of S1 (fit parameters a_i, b_i, ω). The higher degree function was chosen to appropriately represent the asymmetric seasonal cycle introduced by the long and cold winter season. Using (a_1, a_2, b_1, b_2, ω) from the fit and $a_0 = MAT_{1860-1869}$, we generate a time series of air temperatures, which the model is forced with until no more changes in GTs occur.

3.4 Model calibration

In absence of detailed data on the thermal properties of the subsurface (in terms of c, k, ρ and VWC), we empirically determined the values by adjusting until satisfying agreement between model results and available observations over the calibration period. We selected S1 as calibration period, while S2 and S3 were kept as independent control for subsequent model validation (see following section). For calibration, the model was forced by using measured ground surface temperature as upper boundary condition. A ~~careful,~~ stepwise optimization procedure was applied to avoid erroneous parameter calibration which may result from compensating effects. As such, for example, a wrong choice for heat capacity may cause an exaggerated phase shift of GT with respect to GST which in turn may partly be compensated for by enhanced heat conduction. Our approach to deal with this problem was to preselect ranges of plausible values for the parameters from literature (Williams and Smith, 1989). Previous sensitivity testing revealed that within the given bounds, modelled GT were most sensitive to

changes in heat conductivity and water content, while heat capacity and density are robustly constrained by literature values. Therefore, after assignment of plausible starting values to the parameters, calibration was performed by systematically changing k and VWC over the given ranges aiming for improving the agreement between modelled and observed GTs at different depth levels. Subsequently, minor adjustments were made to c_i and ρ to fine-tune the model performance. The agreement between model and observation was quantified at each individual depth in terms of the Nash-Sutcliffe model efficiency coefficient (ME) (Nash and Sutcliffe, 1970). For bedrock, values for thermal conductivity and density were measured at Juv-BH4 and at all sites at Jetta by the Norwegian Geological Survey (NGU), and these observations served as initial guesses for the calibration. A time series of measured soil moisture (O. Humlum, 2011, personal communication) in the vicinity of some sites (Juv-BH1, Tro-BH1) served as an estimate for the water content in the near-surface sediments. Adopted values for the different materials are shown in Table 2, while depth-averaged values of the ME for each borehole are presented in Table 3.

In total, only slight changes to the starting values had to be applied to achieve satisfactory agreement between modelled and observed GT. We defined satisfaction as $\text{ME} > 0.7$ and/or when further changes of parameter values did not yield better model performance. Nevertheless, we emphasize that the obtained set of parameter values for each site represent one possible set that yields satisfactory agreement between model and observations. However, as symptomatic for calibrating numerical models, different sets may exist and calibrated values may be erroneous. Therefore, transferability of parameter values to other regions is restricted and site-specific calibration is necessary.

3.5 Model validation

For our validation procedure we followed Rykiel's (1996) suggestion that the meaning of validation is that a "model is acceptable for its intended use because it meets specified performance requirements" in terms of operational validation. For our study

the correspondence between measured and observed GT is expressed by the depth-averaged values of the Nash-Sutcliffe model efficiency coefficient (ME). Again, we require ME > 0.7.

To validate the reliability of the GST model, it was run for each season individually using the average n-factors from S1 and S2 (Table 1). For most boreholes a good correspondence between modelled and measured GSTs was achieved with ME > 0.8 (Table 3, Fig. 5). Since S3 was not included in the average n-factor calculation, it represents an additional independent validation period. Despite some differences in the snow conditions, the model reproduced GSTs of S3 equally well (Table 3). The highest values of ME > 0.9 were achieved at bedrock sites with negligible winter snow cover (Juv-BH4, Jet-BH3). The measured GTs of the validation period (S2–S3) are well reproduced by the calibrated model yielding ME-values ranging from 0.81 to 0.93 (Table 3).

To better estimate the model performance on a long-term scale, the model was run from 1860 until 2009 using the reconstructed T_{AIR} series and results compared to the measured GTs of S1. In the case of the PACE borehole modelled and measured GTs of the entire series 1999–2009 were compared down to a depth of 100 m. The measured MAGTs were reproduced with a RMSE of 0.6–0.7 °C in the uppermost part (0 to 1 m depth) and 0.1–0.3 °C at a depth between 5 and 10 m (Fig. 7).

4 Results

4.1 Historical and future air temperature trends

The historical air temperature series show temperature increases of 1.4 °C to 2.1 °C (+0.9 °C/100 yr and +1.4 °C/100 yr) between 1860/1870 and 2008/2009 at Juvasshøe and Tron, respectively. During the last decade (2000–2010) only positive deviations of T_{AIR} to the climate normal 1961–1990 were observed all sites (Fig. 8b,c). In the period 1860s until 2000/2009 the strongest warming occurred during spring with +2.1 °C at

both sites. The more continental site Tron, however, shows strong increases of air temperature both in winter as well as in spring with +1.8 and +1.9 °C, respectively.

The median of the downscaled future temperatures indicates a further warming of +2.8 °C of the decadal means 2001/2010 until 2091/2100. The 10th percentile shows the same warming trend, the 90th percentile, however, shows an increase of +3.3 °C (Fig. 8a). The deviation of the median to the climate normal 1961–1990 amounts to +3.8 °C and +4.2 °C at Juvvasshøe (Fig. 8b) and Tron (Fig. 8c), respectively.

4.2 Historic permafrost development

4.2.1 Mountain permafrost after the Little Ice Age

From the initial situation in 1860 rough estimates on the lower altitudinal limit of mountain permafrost after the LIA can be made. The model results suggest the presence of permafrost at Juvvasshøe at c. 1300 m a.s.l. (Juv-BH6). The modelled ALT range from 0.5 m at 1900 m a.s.l. (Juv-BH1) to c. 3 m at 1300 m a.s.l (Juv-BH6). The greatest ALT (close to 4 m) was modelled for the bedrock site (Juv-BH4). At Tron, permafrost thicknesses of up to 90 m and ALT of c. 1.3 m to 6 m were modelled. According to the model results, the altitudinal zone of the lower limit of permafrost at this site was below c. 1300 m a.s.l.

4.2.2 Ground temperatures

According to the model results for the period from 1860 to 2009, GTs were increasing at all depths. At all boreholes, most significant increases in GT occurred in the last two decades (since 1990). The model results show an increase in GT at 10 m depth since the 1860s by about 0.9 °C to 1.5 °C at Juvvasshøe and 0.1 °C to 0.7 °C at Tron. GTs at 100 m depth increased in the range of 0.4 °C to 1.0 °C at Juvvasshøe and 0.1 °C to 0.4 °C at Tron. Modelled warming was strongest for the bedrock borehole (Juv-BH4) with +1.5 °C and +0.5 °C at 10 m and 100 m depth, respectively.

4.2.3 Active layer thickness

Depending on location, elevation and stratigraphy, different ALT behaviour is indicated by the model results. A characteristic pattern is observed at all boreholes, with a comparatively slow ALT increase until the end of the 20th century (1995/1999) and accelerated increase in ALT during the decade 2000–2009.

Trends of ALT increase were derived for the two periods 1860/64–1995/1999 and 2000–2010. The non-parametric Mann-Kendall test was used to test these trends for significance (1 % level). At Juvvasshøe and Jetta all trends of ALT increase during both periods have been proven significant, while at Tron only the trend for the later period (1990–2010) is significant.

At Juvvasshøe the lowermost borehole (Juv-BH6) shows a very rapid ALT increase and permafrost degradation prior to the end of the 19th century. The 20th century increase in ALT at the other boreholes was only +0.2 m (24 %, +0.1 cm yr^{-1}) and +0.7 m (54 %, +0.5 cm yr^{-1}) at Juv-BH1 and PACE (Fig. 9a), respectively. At the lower boreholes (Juv-BH3 and Juv-BH4) an ALT increase of +2.3 m (68 %, +1.6 cm yr^{-1}) and +2.4 m (65 %, +1.7 cm yr^{-1}) was modelled, respectively. The model results indicate a stronger ALT increase at all boreholes during the last 10 yr in the range of +0.2 to +2.6 m (20–46 %, 2–26 cm yr^{-1}). The PACE borehole shows higher mean inter-annual variation of ALT than Juv-BH1 with +40 cm yr^{-1} and +20 cm yr^{-1}, respectively. Although Juv-BH3 was drilled in coarse material and Juv-BH4 in bedrock they show a similar ALT evolution, the latter however, having continuously larger ALT (average +0.4 m) and a much higher mean inter-annual variation of 70 cm yr^{-1} compared to 30 cm yr^{-1}.

As all boreholes are drilled in bedrock at Jetta, the ALT is more sensitive to climate variations, and a more rapid increase during the last 150 yr was modelled. Until 1990 the ALT increased by +1.1 m (26 %, +1 cm yr^{-1}) and +2.2 m (40 %, +2 cm yr^{-1}) at Jet-BH1 and Jet-BH3, respectively. During the period 1990 until 2010 the strongest increase of ALT of +2.7 m (50 %, +14 cm yr^{-1}) was modelled at Jet-BH1, while per-

mafrost degradation was modelled for Jet-BH3 (Fig. 9b).

At Tron the strongest increases in ALT were modelled with +1.1 m (110 %, +0.8 cm yr^{-1}) until the end of the 20th century (Fig. 9c). Within the last decade only, the model indicates a rapid warming of permafrost with an ALT reaching a depth of 10–11 m as measured today. This indicates an ALT increase of nearly +9 m (430 %, +87 cm yr^{-1}) since 1990. This development agrees well with observations indicating the possible beginning of a talik development (Fig. 3c) (Farbrot et al., 2011).

4.3 Future permafrost development

4.3.1 Ground temperatures

According to modelled GT until 2100, warming will continue beyond that found for 2000–2009. The model suggests that GTs at Juv-BH1 will increase by +1.9 °C and +1.1 °C at 30 m and 100 m depth until 2100, respectively. Juv-BH4 shows the same warming at 100 m depth, but a more pronounced increase in GT at 30 m with +2.6 °C.

4.3.2 Active layer thickness

The model results are indicative for permafrost degradation also above 1800 m a.s.l. until 2100. Permafrost at lower elevations (Juv-BH3 and Juv-BH4) degrades completely before 2050 (Fig. 9a). At the bedrock site at Jetta the rapid AL thickening rates at Jet-BH1 will continue and the development of a talik until the end of the 2020s is predicted by the model (Fig. 9b).

While the air temperature increase in the climate change scenario shows a linear development and even a decrease in the warming rate (Fig. 8a), the ALT displays a non-linear response at most sites (Fig. 9). The ALT of Juv-BH1 increases linearly by another 70 cm from 2010 until mid 2070s. Although the climate change scenario includes a decrease in the warming rate at this point, a rapid degradation of permafrost subsequently takes place until the end of this century, with a linear increase of ALT by

Modelling borehole temperatures in Southern Norway

T. Hipp et al.

Title Page

Abstract | Introduction

Conclusions | References

Tables | Figures

◄ | ►

◄ | ►

Back | Close

Full Screen / Esc

Printer-friendly Version

Interactive Discussion

$> 40\,\text{cm}\,\text{yr}^{-1}$. A similar development can be observed at the PACE borehole with higher thickening rates and a permafrost degradation at the mid 2060s.

Running the model with the 90th and 10th percentiles of the downscaled temperature ensemble yields an estimation of the possible range of developments. The 90th percentile causes a fast degradation of permafrost at all boreholes by latest mid of this century (Fig. 9a). Considering the moderate warming projections (10th percentile), permafrost at Juv-BH1 and PACE is warming at a slow rate without degradation occurring.

4.3.3   Probable future of permafrost at the PACE and Juv-BH1 boreholes

Concerning the projected air temperate, there are uncertainties related to the different formulations of the GCMs themselves, as well as to the empirical-statistical downscaling procedure (Benestad, 2011). Although only one emission scenario is considered here (A1b), the uncertainties lead to considerable spread of projected temperature. In order to quantify the effects of this uncertainty on modelled ALT and GT, the development of GT and ALT until 2100 were simulated for all percentiles of the projected T_{AIR}-ensemble in steps of 5 %. From these results, we identify the percentiles which are associated with disappearance of an AL in the years 2050 and 2100, respectively. This analysis is used to estimate the probabilities for transition of permafrost to talik at Juv-BH1 and PACE in the years 2050 and 2100 (Fig. 10).

For the PACE borehole, a talik evolution until 2100 was modelled already using the 25th percentile resulting in a high probability of 70–75 % (Fig. 9). According to the classification proposed by the IPCC (IPCC, 2007), this situation is therefore *likely* to occur for the given emission scenario. However, at Juv-BH1 a talik will have developed in 2100 with a probability of 50–55 %, and is classified *as likely to occur as not*. The probabilities for talik evolution until 2050 is 35–40 % for PACE and 20–25 % for Juv-BH1, respectively and therefore *unlikely* (Fig. 10). According to these model results, above 1800 m a.s.l, where stable and continuous mountain permafrost is found today,

Modelling borehole temperatures in Southern Norway

T. Hipp et al.

Title Page

Abstract	Introduction
Conclusions	References
Tables	Figures

◄◄   ►►

◄   ►

Back   Close

Full Screen / Esc

Printer-friendly Version

Interactive Discussion

discontinuous mountain permafrost is to be expected by the end of the 21st century.

5 Discussion

5.1 Model uncertainties due to snow cover, soil water content variability and model approach

A major source of uncertainty is related to the parameterisation of using constant n-factors. It is uncertain how well the snow conditions of the historic and future model period are represented by the average n-factor from S1 and S2. A 10-yr record (1999–2008) of GST and T_{AIR} is available at the PACE borehole (Isaksen et al., 2011), which enables an estimate for the decadal variation of n-factors and put the period 2008–2010 into context. A mean n_F-factor of 0.91 (0.89–0.98) and n_T-factor of 1.12 (1.02–1.26) was derived from the records. The mean n_F- and n_T-factors for 2008–2010 (Table 1) therefore are within the variation of the period 1999–2009. Additionally, based on these minimum and maximum values an uncertainty analysis was conducted to give a quantitative estimate on the error that can be expected from n-factors that do not accurately represent the actual snow cover. For that purpose, the model was run for the PACE borehole for 1999–2010 separately both with the minimum and maximum n-factors. This implies running the model with the coldest ($n_F = 0.98$; $n_T = 1.02$) and warmest ($n_F = 0.89$; $n_T = 1.26$) possible GST conditions. The differences in GTs expressed in the absolute error between the two model runs were calculated for each depth individually. A change in ALT of < 50 cm and changes in MAGT of 0.7 °C to 0.4 °C at the surface and 10 m depth, respectively, were introduced. The PACE borehole represents a site with relatively constant n_F-factors due to the negligible snow cover. At sites with higher snow cover and thus smaller n_F-factors (particularly Tr-BH2, Jet-BH1 and Tr-BH6), our measurements suggest a higher interannual variability of the n_F-factors (Table 1), most likely caused by different wind redistribution of snow. However, the good agreement of modelled long-term subsurface temperatures with measured GT gives us confidence

Title Page

Abstract | Introduction

Conclusions | References

Tables | Figures

◄◄ | ►►

◄ | ►

Back | Close

Full Screen / Esc

Printer-friendly Version

Interactive Discussion

that the *n*-factors assumed in the model runs are a good representation of long-term average *n*-factors.

Some deviations of modelled from observed GTs are observed during periods of thawing and freezing, presumably caused by our assumption of constant VWC. At sites where VWC > 15 %, the model typically underestimates the pronounced zero-curtain effect observed. (Fig. 5). Further, our model neglects advective heat transport, and changes of ice-content in the ground are not recognised in the model. The degradation of permafrost would remove ice and enhance water drainage, leading to an increased warming in the ground. This process is observed at Juv-BH5 and discussed in more detail by Farbrot et al. (2011) (see also Isaksen, 2011). Our modelling does not account for this process and therefore, rather represents a minimum estimate for the increase of GT.

A third process not included in the model are 3-D-effects due to lateral variation of either topography or snow cover. Farbrot et al. (2011) suggests that 3-D-effects may affect BH5 due to variable snow cover. In our 1-D modelling this effect is probably compensated for by the calibration parameters, so that the performance of the model is relatively good. Hence, the results for BH5 in deeper soil layers should be treated with caution.

The aim of this study are to assess the long-term trends of permafrost temperature and its altitudinal distribution. We assume conduction and latent heat effects as main factors, which is in agreement with studies showing that conduction and latent heat effects attribute for most of the heat flow processes (Kane et al., 2001; Weismüller et al., 2011). Both soil water/ice content and snow conditions on the long-term are afflicted with uncertainties. For this study we suggest that the average *n*-factor value we used provides a useful approximation to address the snow influence on GST. The constancy of soil water content may be responsible for slight deviations during periods of zero-curtain. Nevertheless, observed GT, ALT and GT amplitudes were reproduced reasonably well according to the ME measure used in this study. Long-term data are not available, which e.g. could aid possible trends of *n*-factors or soil water content, so

we do not know if and how trends and inter-annual variations would interfere with each other and affect our result. Moreover, at our sites and generally in most high-mountain settings in Scandinavia, coarse-grained near-surface material or bedrock is dominating. Thus, the soil water content is relatively low and the effect of water flow on GT is considered minor. Furthermore, the boreholes have been drilled in flat topography, in doing so, 3-D-effects are largely avoided. Processes of lateral heat transfer along a slope and air convection within the pore space of block fields seem not important.

Even with the stated simplifications, modelled GTs agree well with observations and the present borehole temperature distributions are reproduced when simulating the evolution since 1870. These results suggest therefore, that our simple approach is capable of capturing the dominating processes within the time scale considered.

5.2 Uncertainties of reconstructed and projected air temperature series

The method by Hanssen-Bauer and Nordli (1998) has proven useful in reconstructing reliable air temperature time series (Farbrot and Hanssen-Bauer, 2009). However, it introduces uncertainty due to the spatial and temporal interpolation of air temperatures.

Before daily values become available in 1957, the model is run with monthly data. To test the possible error introduced by the discontinuity in temporal resolution, the period 2008–2010 was simulated with monthly means. The model result does not show any significant deviation to those obtained when using the daily resolution input data.

Uncertainties related to the interpolation in mountain topography arise from unknown lapse rates during inversions (Tveito and Førland, 1999), which are observed frequently, especially during calm winter days. The temperature fields used in this study for the long-term record are based on constant lapse rates, which may produce too cold SAT in high elevations (e.g., Tveito and Førland, 1999). However, generally a good fit has been achieved when comparing measured and interpolated air temperature, indicating the mean temperature trends being well represented (Tveito and Førland, 1999).

In our study we employ ensemble estimates of future T_{AIR} evolution to illustrate and assess the uncertainty of the future GT evolution. Ensemble analysis has proven pow-

erful in assessing uncertainties of projected T_{AIR} evolution. However, there are several ways to define an ensemble, each of which refers to a different cause of uncertainty. In detail, the ensemble may consist of GCM realizations for a multitude of emission scenarios, thereby uncovering the range of expected outcomes for the discrete emission scenarios defined by IPCC (2007). Furthermore, a T_{AIR} ensemble may also consist of many realizations for one single emission scenario but from a multitude of GCMs. The combination of both would also be possible, though we regard that possibility as little instructive. Here, we have focused on illustrating the uncertainty related to the choice of GCM for a given scenario rather than on the uncertainty related to future emissions. Namely, we have chosen the A1b scenario for which empirically-statistically downscaled time series of T_{AIR} are available for a multi-model ensemble (Benestad, 2011).

5.3 Influence of ground properties on thermal regime

GTs respond differently to warming, depending on the surface material, ground properties and soil water content. The inter-annual change of ALT was calculated and averaged for the period 1860–2009 for all boreholes at Juvvasshøe. Borehole Juv-BH4, which does not have significant snow cover and is located in bedrock, shows the highest variation of 0.7 m yr^{-1}. Much lower inter-annual ALT variations of 0.2–0.3 m yr^{-1} were modelled for boreholes covered by block fields. This reflects how the block fields act as a buffer dampening the effect of the air temperature fluctuations on GT (Harris and Pedersen, 1998; Juliussen and Humlum, 2008). At Juv-BH4, however, no such buffer layer exists causing a more direct response of the ALT to changes in T_{AIR}.

Despite their proximity, the boreholes PACE and Juv-BH1 show different thermal regimes and ALT developments in past and future due to differences in volumetric water content. A large part of the energy transferred into the ground at Juv-BH1 is consumed for melting ground ice. This explains the reduced inter-annual variability of ALT and the less pronounced increase in ALT in the past and future. Furthermore, the non-linear response in ALT is attributed to the melting of ice within the ground.

Modelling borehole temperatures in Southern Norway

T. Hipp et al.

After melting of ground ice, more energy is available to efficiently warm the ground. Similar effects have been observed in North-America (Smith et al., 2010) and Russia (Romanovsky et al., 2010), where the non-linear response of GT and ALT to warming are clearly attributable to water content. Similar results have been found comparing the impact of the extreme summer of 2003 on the ALT of bedrock and block field sites in the Swiss Alps (Vonder Mühll et al., 2007).

Several other studies have attempted to quantify the impact of climate change on permafrost conditions, distribution and ALT. Stendel and Christensen (2002) predicted a general increase of ALT of up to 30–40 % until the end of the 21st century in the Northern Hemisphere. Zhang et al. (2008) estimated the ALT increase in Canada to 14–30 % by 2050 compared to a permafrost baseline in the 1990s. For Svalbard, similar changes for the ALT evolution during the 21st century were modelled (Etzelmüller et al., 2011). In our study the ALT increased by 65 % to 180 % at the boreholes where permafrost still is expected by 2050. Even the results using the 10th percentile of the climate change models indicate an ALT increase of 44 % at the PACE borehole. This implies a high sensitivity of warm mountain permafrost to climate change, comparable to coastal areas e.g. on Svalbard (Etzelmüller et al., 2011). Furthermore, many of the assessments mentioned above were made for Arctic lowlands, where large areas with fine-grained and organic-rich sediments are present. Organic components in the near-surface layer are known to effectively damp the GT response to warming (Williams and Smith, 1989). In mountain areas, significant accumulation of organic material is seldom and restricted to special topographic and geomorphic settings. However, block fields may have an effect similar to that of organic material in Arctic lowlands, i.e. retarding the GT-response to climate signals and cooling the ground, as discussed above.

In summary our modelling study shows a high sensitivity of mountain permafrost and high probabilities of degradation at elevation levels below c. 1800 m a.s.l. in Southern Norway. Simulated GTs at bedrock sites are generally more sensitive to climate change than those at sites within block fields or finer-grained sediment cover.

5.4 Altitudinal changes of mountain permafrost during the modelling period

This study indicates a major change in ground thermal regime since the end of the LIA. At that time, sporadic to discontinuous permafrost conditions seem to have been more widespread at elevations of around 1300 m a.s.l., where we only find permafrost as isolated patches at present (Sollid et al., 2003). This translates to the lower permafrost zone being approximately 200 m lower during the LIA than at present. At Juvvasshøe, this zone between 1300 m a.s.l. up to 1500 m a.s.l. is dominated by block lobes, which may be inactive today, but are shaped by an earlier high-active periglacial environment. Further climate warming would move this zone up-slope. The model results of this study indicate that the lower limit of the discontinuous permafrost zone may rise up to above 1800 m a.s.l., thus, c. 250 m higher than today. With such a scenario, major changes in periglacial processes are expected.

As our results are derived from 1-D modelling at the point scale, these implications on the spatial distribution of mountain permafrost have to be treated with care. The large spatial heterogeneity of parameters that strongly influence permafrost distribution such as snow cover, surface cover and ground parameters ~~can not be~~ considered in these estimations, as recently documented by Gubler et al. (2011) for sites in Switzerland and Etzelmüller et al. (2007) in Iceland. Therefore, a simple point-to-area extrapolation is problematic. However, we have three main reasons to consider this set-up as sufficient to give estimations on the altitudinal changes of mountain permafrost since the LIA in these very particular mountain areas: (1) The 13 boreholes cover a large altitudinal range from 1900 m a.s.l. to c. 1200 m a.s.l., today ranging from continuous permafrost to no permafrost, (2) Farbrot et al. (2011) clearly documented consistent altitudinal trends in GT on an annual average and (3) even if a borehole location is not representative for the local variability of surface characteristics, the GT signal in greater depth will be integrated over a larger surface area.

Title Page

Abstract | Introduction

Conclusions | References

Tables | Figures

◄◄ | ►►

◄ | ►

Back | Close

Full Screen / Esc

Printer-friendly Version

Interactive Discussion

6 Conclusions and perspectives

From this study we draw the following conclusions:

- Forcing the model with reconstructed T_{AIR} over 1860–2009 yielded vertical profiles of GT close to those observed in 2009, thereby suggesting validity of our approach.

- During the Little Ice Age the altitudinal zone covering the lower limit of permafrost was approximately 200 m lower than today in the field area. A future warming according to the A1B scenario would further lift this zone by c. 250 m towards the end of the 21st century, depending on site characteristics and snow cover development.

- Model results suggest that GT at 10 m depth increased by $+0.9\,^{\circ}\text{C}$ to $+1.5\,^{\circ}\text{C}$ over 1860–2009. The largest part of this warming occurred after 1990.

- From 1860 until c. 1990 a comparatively small increase in active layer thickness was modelled where permafrost exists, with values ranging from $0.1\,\text{cm}\,\text{yr}^{-1}$ to $+2\,\text{cm}\,\text{yr}^{-1}$ (20–68 %). Since c. 1990 ALT-change rates of $+2\,\text{cm}\,\text{yr}^{-1}$ to $+87\,\text{cm}\,\text{yr}^{-1}$ (20–430 %) were modelled. The model results indicate permafrost degradation at boreholes below c. 1450–1500 m at Juvvasshøe and Jetta and below c. 1600 at Tron.

- Throughout the 21st century degradation of permafrost at most of the sites below c. 1800 m a.s.l. is suggested by the model. By the end of this century the highest locations (Juv-BH1, PACE) will experience pronounced ALT-increases of up to 10 m or the development of taliks. This implies an upward shift of the lower permafrost zone to around 1800 m a.s.l. by the end of the 21st century, again depending on sediment characteristics and snow cover development.

- Our study successfully simulated the non-linear response of ground temperature and active layer thickness to increasing air temperatures, due to the thermal iner-

tia of ice-containing ground material. In our sites, this response is related mainly to block fields and coarse ground moraine sites containing ice.

The modelled past and possible future changes in GT and ALT have geomorphologic and geotechnical implications since the ground thermal regime is a major controlling factor for geomorphologic processes and landscape development (Berthling and Etzelmüller, 2011). As alpine rock faces are widespread in the study area between 1900 and 2400 m a.s.l, our study suggests major impacts on the geotechnical properties and stability of rock walls. This relationship is well-documented in literature (Davies et al., 2001; Gruber et al., 2004a) and has to be evaluated in future research. Especially the modelled long period of stable permafrost and a subsequent sudden and quick degradation results in challenges for engineering, natural hazard prediction and mitigation. Finally, our study provides important insights in the range of thermo-physical parameters in a wide range of bedrock and surficial material relevant for mountain areas in Southern Norway. These provide important constraints for spatial numerical permafrost modelling.

References

Benestad, R. E.: Climate change scenarios for Northern Europe from multi-model IPCC AR4 climate simulations, Geophys. Res. Lett., 32, L17704, doi:10.1029/2005GL023401, 2005.

Benestad, R. E.: A new global set of downscaled temperature scenarios, J. Climate, 24, 2080–2098, doi:10.1175/2010JCLI3687.1, 2011.

Berthling, I. and Etzelmüller, B.: The concept of cryo-conditioning in landscape evolution, Quaternary Res., 75, 378–384, doi:10.1016/j.yqres.2010.12.011, 2011.

Biesinger, Z., Rastetter, E. B., and Kwiatkowski, B. L.: Hourly and daily models of active layer evolution in arctic soils, Ecol. Model., 206, 131–146, 2007.

Burn, C. R. and Zhang, Y.: Permafrost and climate change at Herschel Island (Qikiqtaruq), Yukon Territory, Canada, J. Geophys. Res.-Earth, 114, F02001, doi:10.1029/2008JF001087, 2009.

Bø, M. R.: Permafrost studies on Jetta in Northern Gudbrandsdalen, Central Norway (in Norwegian), Master's thesis, University of Oslo, 127 pp., 1998.

Christiansen, H. H., Etzelmuller, B., Isaksen, K., Juliussen, H., Farbrot, H., Humlum, O., Johansson, M., Ingeman-Nielsen, T., Kristensen, L., Hjort, J., Holmlund, P., Sannel, A. B. K., Sigsgaard, C., Akerman, H. J., Foged, N., Blikra, L. H., Pernosky, M. A., and Odegard, R. S.: The thermal state of permafrost in the nordic area during the international polar year 2007–2009, Permafrost Periglac., 21, 156–181, doi:10.1002/Ppp.687, 2010.

Davies, M. C. R., Hamza, O., and Harris, C.: The effect of rise in mean annual temperature on the stability of rock slopes containing ice-filled discontinuities, Permafrost Periglac., 12, 137–144, doi:10.1002/ppp.378, 2001.

Engelhardt, M., Hauck, C., and Salzmann, N.: Influence of atmospheric forcing parameters on modelled mountain permafrost evolution, Meteorol. Z., 19, 491–500, doi:10.1127/0941-2948/2010/0476, 2010.

Etzelmüller, B., Farbrot, H., Gudmundsson, A., Humlum, O., Tveito, O. E., and Bjornsson, H.: The regional distribution of mountain permafrost in Iceland, Permafrost Periglac., 18, 185–199, doi:10.1002/Ppp.583, 2007.

Etzelmüller, B., Schuler, T. V., Isaksen, K., Christiansen, H. H., Farbrot, H., and Benestad, R.: Modeling the temperature evolution of Svalbard permafrost during the 20th and 21st century, The Cryosphere, 5, 67–79, doi:10.5194/tc-5-67-2011, 2011.

Farbrot, H. and Hanssen-Bauer, I.: A simple staion-based empirical model for local snow con-

ditions, Norwegian Meteorological Institute, met.no Report 3/2009, http://met.no/Forskning/Publikasjoner/Publikasjoner_2009/filestore/metnoRapport3_2009_mod.pdf, 2009.

Farbrot, H., Etzelmüller, B., Schuler, T. V., Gudmundsson, A., Eiken, T., Humlum, O., and Bjornsson, H.: Thermal characteristics and impact of climate change on mountain permafrost in Iceland, J. Geophys. Res.-Earth, 112, F03S90, doi:10.1029/2006jf000541, 2007.

Farbrot, H., Hipp, T., Etzelmüller, B., Isaksen, K., Ødegård, R. S., Schuler, T. V., and Humlum, O.: Air and ground temperature variations observed along elevation and continentality gradients in Southern Norway, Permafrost Periglac., 22, 343–360, doi:10.1002/ppp.733, 2011.

Fischer, L., Kääb, A., Huggel, C., and Noetzli, J.: Geology, glacier retreat and permafrost degradation as controlling factors of slope instabilities in a high-mountain rock wall: the Monte Rosa east face, Nat. Hazards Earth Syst. Sci., 6, 761–772, doi:10.5194/nhess-6-761-2006, 2006.

Gude, M. and Barsch, D.: Assessment of geomorphic hazards in connection with permafrost occurrence in the Zugspitze area (Bavarian Alps, Germany), Geomorphology, 66, 85–93, doi:10.1016/j.geomorph.2004.03.013, 2005.

Gruber, S. and Hoelzle, M.: The cooling effect of coarse blocks revisited: a modeling study of a purely conductive mechanism, 9th International Conference on Permafrost, Fairbanks, Alaska, 2008.

Gruber, S., Hoelzle, M., and Haeberli, W.: Permafrost thaw and destabilization of Alpine rock walls in the hot summer of 2003, Geophys. Res. Lett., 31, L13504, doi:10.1029/2004gl020051, 2004a.

Gruber, S., Hoelzle, M., and Haeberli, W.: Rock-wall temperatures in the Alps: modelling their topographic distribution and regional differences, Permafrost Periglac., 15, 299–307, doi:10.1002/ppp.501, 2004b.

Gubler, S., Fiddes, J., Keller, M., and Gruber, S.: Scale-dependent measurement and analysis of ground surface temperature variability in alpine terrain, The Cryosphere, 5, 431–443, doi:10.5194/tc-5-431-2011, 2011.

Haeberli, W.: Construction, environmental problems and natural hazards in periglacial mountain belts, Permafrost Periglac., 3, 111–124, 1992.

Hanssen-Bauer, I.: Regional temperature and precipitaion series for Norway: analyses of time-series updated to 2004, Norwegian Meteorological Institute, 2005.

Hanssen-Bauer, I. and Nordli, P. Ø.: Annual and seasonal temperature variations in Norway

Modelling borehole temperatures in Southern Norway

T. Hipp et al.

1876–1997, DNMI Report, Norwegian Meteorological Institute, 1998.

Harris, C., Haeberli, W., Vonder Mühll, D., and King, L.: Permafrost monitoring in the high mountains of Europe: the PACE Project in its global context, Permafrost Periglac., 12, 3–11, doi:10.1002/ppp.377, 2001.

5 Harris, C., Arenson, L. U., Christiansen, H. H., Etzelmüller, B., Frauenfelder, R., Gruber, S., Haeberli, W., Hauck, C., Hölzle, M., Humlum, O., Isaksen, K., Kääb, A., Kern-Lütschg, M. A., Lehning, M., Matsuoka, N., Murton, J. B., Nötzli, J., Phillips, M., Ross, N., Seppälä, M., Springman, S. M., and Vonder Mühll, D.: Permafrost and climate in Europe: monitoring and modelling thermal, geomorphological and geotechnical responses, Earth-Sci. Rev., 92, 10 117–171, doi:10.1016/j.earscirev.2008.12.002, 2009.

Harris, S. A. and Pedersen, D. E.: Thermal regimes beneath coarse blocky materials, Permafrost Periglac., 9, 107–120, doi:10.1002/(sici)1099-1530(199804/06)9:2<107::aid-ppp277>3.0.co;2-g, 1998.

Hoelzle, M., Mittaz, C., Etzelmüller, B., and Haeberli, W.: Surface energy fluxes and distribution 15 models of permafrost in european mountain areas: an overview of current developments, Permafrost Periglac., 12, 53–68, 2001.

Huggel, C., Salzmann, N., Allen, S., Caplan-Auerbach, J., Fischer, L., Haeberli, W., Larsen, C., Schneider, D., and Wessels, R.: Recent and future warm extreme events and high-mountain slope stability, Philos. T. Roy. Soc. A, 368, 2435–2459, doi:10.1098/rsta.2010.0078, 2010.

20 IPCC: Summary for Policymakers, in: Climate Change 2007: The Physical Science Basis. Contribution of Working Group I to the Fourth Assessment Report of the Intergovernmental Panel on Climate Change, edited by: Solomon, S., Qin, D., Manning, M., Chen, Z., Marquis, M., Averyt, K. B.,Tignor, M., and Miller, H. L., Cambridge University Press, Cambridge, UK and New York, NY, USA, 2007.

25 Isaksen, K., Vonder Muhll, D., Gubler, H., Kohl, T., and Sollid, J. L.: Ground surface-temperature reconstruction based on data from a deep borehole in permafrost at Janssonhaugen, Svalbard, Ann. Glaciol., 31, 287–294, 2000.

Isaksen, K., Holmlund, P., Sollid, J. L., and Harris, C.: Three deep alpine-permafrost boreholes in Svalbard and Scandinavia, Permafrost Periglac., 12, 13–25, 2001.

30 Isaksen, K., Hauck, C., Gudevang, E., Ødegård, R. S., and Sollid, J. L.: Mountain permafrost distribution on Dovrefjell and Jotunheimen, Southern Norway, based on BTS and DC resistivity tomography data, Norsk Geogr. Tidsskr., 56, 122–136, 2002.

Isaksen, K., Heggem, E. S. F., Bakkehoi, S., Odegard, R. S., Eiken, T., Etzelmuller, B., and

Sollid, J. L.: Mountain permafrost and energy balance on Juvvasshoe, Southern Norway, 8th International Conference on Permafrost, Zurich, Switzerland, ISI:000185049300083, 467–472, 2003.

Isaksen, K., Benestad, R. E., Harris, C., and Sollid, J. L.: Recent extreme near-surface permafrost temperatures on Svalbard in relation to future climate scenarios, Geophys. Res. Lett., 34, L17502, doi:10.1029/2007gl031002, 2007.

Isaksen, K., Ødegård, R. S., Etzelmüller, B., Hilbich, C., Hauck, C., Farbrot, H., Eiken, T., Hygen, H. O., and Hipp, T.: Degrading mountain permafrost in Southern Norway: spatial and temporal variability of mean ground temperatures, 1999–2009, Permafrost Periglac., 22, 361–377, doi:10.1002/ppp.728, 2011.

Juliussen, H. and Humlum, O.: Thermal regime of openwork block fields on the mountains Elgåhogna and Sølen, Central-Eastern Norway, Permafrost Periglac., 19, 1–18, doi:10.1002/ppp.607, 2008.

Kane, D., Hinkel, K. M., Goering, D., Hinzman, L., and Outcalt, S.: Non-conductive heat transfer associated with frozen soils, Global Planet. Change, 29, 275–292, 2001.

Lewkowicz, A. G.: Evaluation of miniature temperature-loggers to monitor snowpack evolution at mountain permafrost sites, Northwestern Canada, Permafrost Periglac., 19, 323–331, 2008.

Luetschg, M., Lehning, M., and Haeberli, W.: A sensitivity study of factors influencing warm/thin permafrost in the Swiss Alps, J. Glaciol., 54, 696–704, doi:10.3189/002214308786570881, 2008.

Lunardini, V. J.: Theory of N-factors., Third International Conference on Permafrost, Edmonton, Canada, 1978.

Malevsky-Malevich, S. P., Molkentin, E. K., Nadyozhina, E. D., and Shklyarevich, O. B.: Numerical simulation of permafrost parameters distribution in Russia, Cold Reg. Sci. Technol., 32, 1–11, 2001.

Mohr, M.: Comparison of Versions 1.1 and 1.0 of Gridded Temperature and Precipitation Data for Norway, Norwegian Meteorological Institute, 2009.

Nash, J. E. and Sutcliffe, J. V.: River flow forecasting through conceptual models part I – a discussion of principles, J. Hydrol., 10, 282–290, 1970.

Noetzli, J. and Gruber, S.: Transient thermal effects in Alpine permafrost, The Cryosphere, 3, 85–99, doi:10.5194/tc-3-85-2009, 2009.

Noetzli, J., Gruber, S., Kohl, T., Salzmann, N., and Haeberli, W.: Three-dimensional distribution

Yoshikawa, K., and Throop, J.: Thermal state of permafrost in North America: a contribution to the international polar year, Permafrost Periglac., 21, 117–135, doi:10.1002/ppp.690, 2010.

Smith, M. W. and Riseborough, D. W.: Climate and the limits of permafrost: a zonal analysis, Permafrost Periglac., 13, 1–15, doi:10.1002/ppp.410, 2002.

Sollid, J. L., Isaksen, K., Eiken, T., and Ødegård, R. S.: The transition zone of mountain permafrost on Dovrefjell, Southern Norway, Eight International Conference on Permafrost, Zurich, Switzerland, 2003.

Stendel, M. and Christensen, J. H.: Impact of global warming on permafrost conditions in a coupled GCM, Geophys. Res. Lett., 29, 1632, doi:10.1029/2001gl014345, 2002.

Stocker-Mittaz, C., Hoelzle, M., and Haeberli, W.: Modelling alpine permafrost distribution based on energy-balance data: a first step, Permafrost Periglac., 13, 271–282, doi:10.1002/ppp.426, 2002.

Tveito, O. E. and Førland, E. J.: Mapping temperatures in Norway applying terrain information, geostatistics and GIS, Norsk Geogr. Tidsskr., 53, 202–212, 1999.

Vonder Mühll, D., Noetzli, J., Roer, I., Makowski, K., and Delaloye, R.: Permafrost in Switzerland 2002/2003 and 2003/2004, Glaciological Report (Permafrost) No. 4/5 of the Glaciological Commission of the Swiss Academy of Sciences (SAS) and the Department of Geography, University of Zurich, 2007.

Weismüller, J., Wollschläger, U., Boike, J., Pan, X., Yu, Q., and Roth, K.: Modeling the thermal dynamics of the active layer at two contrasting permafrost sites on Svalbard and on the Tibetan Plateau, The Cryosphere, 5, 741–757, doi:10.5194/tc-5-741-2011, 2011.

Williams, P. J. and Smith, W.: The Frozen Earth, Cambridge University Press, 1989.

Zhang, Y., Chen, W. J., and Riseborough, D. W.: Temporal and spatial changes of permafrost in Canada since the end of the Little Ice Age, J. Geophys. Res.-Atmos., 111, D22103, doi:10.1029/2006JD007284, 2006.

Zhang, Y., Chen, W. J., and Riseborough, D. W.: Transient projections of permafrost distribution in Canada during the 21st century under scenarios of climate change, Global Planet. Change, 60, 443–456, 2008.

Modelling borehole temperatures in Southern Norway

T. Hipp et al.

Title Page

Abstract	Introduction
Conclusions	References
Tables	Figures

Back | Close

Full Screen / Esc

Printer-friendly Version

Interactive Discussion

Modelling borehole temperatures in Southern Norway

T. Hipp et al.

Title Page

Abstract | Introduction

Conclusions | References

Tables | Figures

◀◀ | ▶▶

◀ | ▶

Back | Close

Full Screen / Esc

Printer-friendly Version

Interactive Discussion

Table 1. Thermal conditions at individual boreholes included in the modelling study, showing mean annual air temperature (MAAT), mean annual ground surface temperature (MAGST) and ground temperature at 10 m depth (MGT_{10}). N_F- and n_T-factors for the two seasons 2008/2009 (S1) and 2009/2010 (S2) and the average (AVG) used in the modelling are shown. For 2010/2011 (S3) only n_F-factors could be calculated due to missing data for the summer months.

Borehole	Elevation [m a.s.l.]	MAAT S1	MAAT S2	MAGST S1	MAGST S2	MGT_{10} S1	MGT_{10} S2	n_F S1	n_F S2	n_F S3	n_F AVG	n_T S1	n_T S2	n_T AVG
JUVVASSHØE														
PACE	1894	−3.4	−4.6	−2.8	−2.9	−2.5	–	0.93	–	–	**0.90^2**	1.17	–	**1.10^2**
BH1	1851	−3.3	−4.7	−2.4	−2.6	−1.6	−1.7	0.88	0.64	0.85	**0.76**	1.18	0.99	**1.09**
BH3	1561	−1.7	−3.1	−0.6	−1.2	−0.3	−0.5	0.96	0.73	0.86	**0.85**	1.52	1.32	**1.42**
BH4	1559	−1.7	−3.1	−1.1	−2.6	–	−0.7	1.03	1.00	0.99	**1.02**	1.38	1.24	**1.31**
BH6	1307	−0.6	−2.2	1.9	0.8	1.7	1.5	0.23	0.34	0.38	**0.29**	1.01	0.96	**0.99**
TRON														
BH1	1640	−3.6	−4.5	0.8	−0.2	0.0	0.0	0.14	0.28	–	**0.21**	1.12	1.04	**1.08**
BH2	1589	−3.0	−3.9	1.1	0.3	0.9	0.8	0.16	0.26	0.40	**0.21**	1.19	1.07	**1.13**
JETTA														
BH1	1560	−2.2	−3.7	−0.4	−0.2	−0.8	−0.8	–	0.37	0.69	**0.37^2**	–	0.98	**1.08^2**
BH3	1218	−0.2	−1.6	0.5	−1.0	1.7_1	1.6_1	0.96	0.99	0.96	**0.98**	1.22	1.21	**1.22**

[1] 9.5 m depth.
[2] Estimated during calibration process due to missing data.

Table 2. Ground properties for different substrates, surface cover and bedrock type, used in the model. Variations within these generalised surface and subsurface classes at different sites can still be found, thus, ranges of parameter values are given. Here, k is thermal conductivity, c is specific heat capacity, VWC is the volumetric water content and ρ is the density.

	k [W K^{-1} m^{-1}]	c [J kg^{-1} K^{-1}]	VWC [%]	ρ [kg m^{-3}]
Block field	0.8–1.4	800	5–20	1200–1600
Vegetated surface layer	0.8	800	14–15	1000–1300
Coarse grained material	1.8–2.3	800	4	1400–2000
Fine moraine material	1.0–1.8	800	4–8	1500–1800
Bedrock	2.7	900	1	2600

Table 3. Model performance in terms of ground surface temperature (GST), ground temperature (GT) and active layer thickness (ALT) at boreholes included in the modelling study. Model performance for GST and GT is expressed in terms of Nash-Sutcliffe model efficiency. Modelled and observed ALT are presented in absolute values. For GT, both the calibration (C) and the validation (V) periods are listed. For the GST the model was run with the averaged n-factors and ME calculated for each season individually.

	GST			GT		ALT_{meas} [m]	ALT_{mod} [m]
	S1	S2	S3	C	V	S1 / S2 / S3	S1 / S2 / S3
JUVVASSHØE							
PACE	0.89	0.85	–	0.88	0.84	2.2 / 2.3 / –	2.1 / 2.1 / –
BH1	0.89	0.86	0.89	0.84	0.82	1.4 / 1.5 / 1.6	1.4 / 1.3 / 1.2
BH3	0.88	0.86	0.92	0.90	0.89	8.5 / 6.8 / 5.6	8.2 / 6.4 / 5.4
BH4	–	0.92	0.96	0.99[*]	0.93[*]	– / 8.6 / 6.6	– / 8.4 / 6.7
BH6	0.91	0.88	0.89	0.92	0.90	–	–
TRON							
BH1	0.71	0.81	–	0.92	0.89	10.7 / 11.1 / –	11.7 / 10.7 / –
BH2	0.90	0.92	0.80	0.85	0.82	–	–
JETTA							
BH1	0.87	0.85	0.80	0.91	0.90	8.0 / 7.3 / 6.9	8.1 / 7.9 / 6.7
BH3	0.96	0.95	0.91	0.95	0.93	–	–

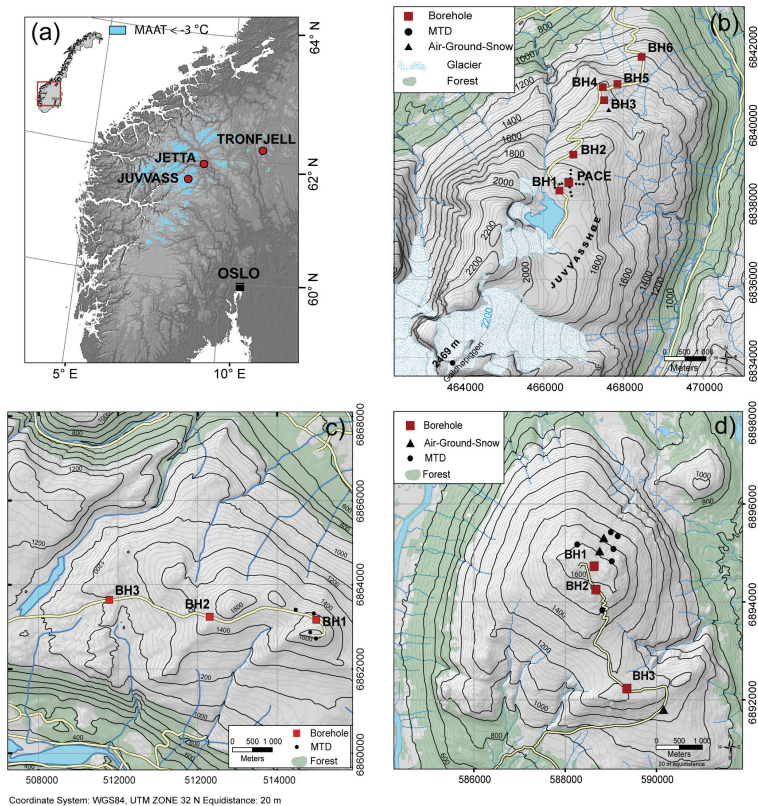[*] Calibration: S2; Validation: S3.

Fig. 1. Location of the study sites and boreholes in Norway **(a)**. As a rough estimate of possible permafrost distribution all areas with MAAT < −3 °C during the last normal period 1961–1990 are shown in blue (Etzelmüller et al., 2003). Local site overview of **(b)** Juvvasshøe, **(c)** Jetta and **(d)** Tron, each indicating the locations of boreholes (BH), where GST measurements (MTD) and T_{AIR}, GST and snow depth measurements are performed.

Title Page

Abstract | Introduction

Conclusions | References

Tables | Figures

|◄ | ►|

◄ | ►

Back | Close

Full Screen / Esc

Printer-friendly Version

Interactive Discussion
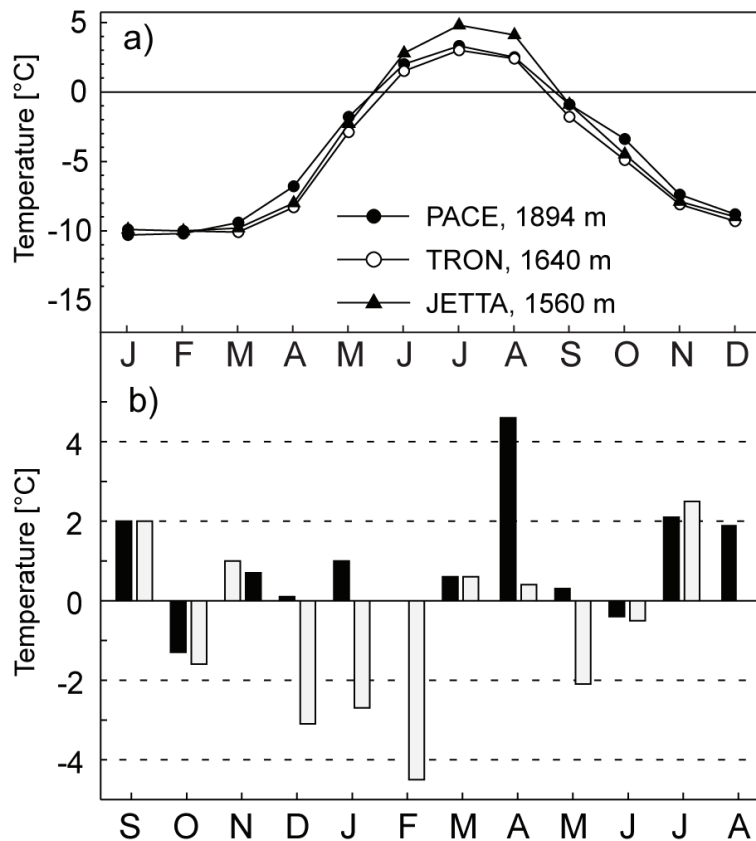
Fig. 2. (a) Mean monthly air temperatures for the PACE borehole at Juvvasshøe, Tron-BH1 and Jet-BH1 during the last normal period 1961–1990. **(b)** Monthly temperature deviations from the normal 1961–1990 at the PACE borehole for S1 (black) and S2 (grey).
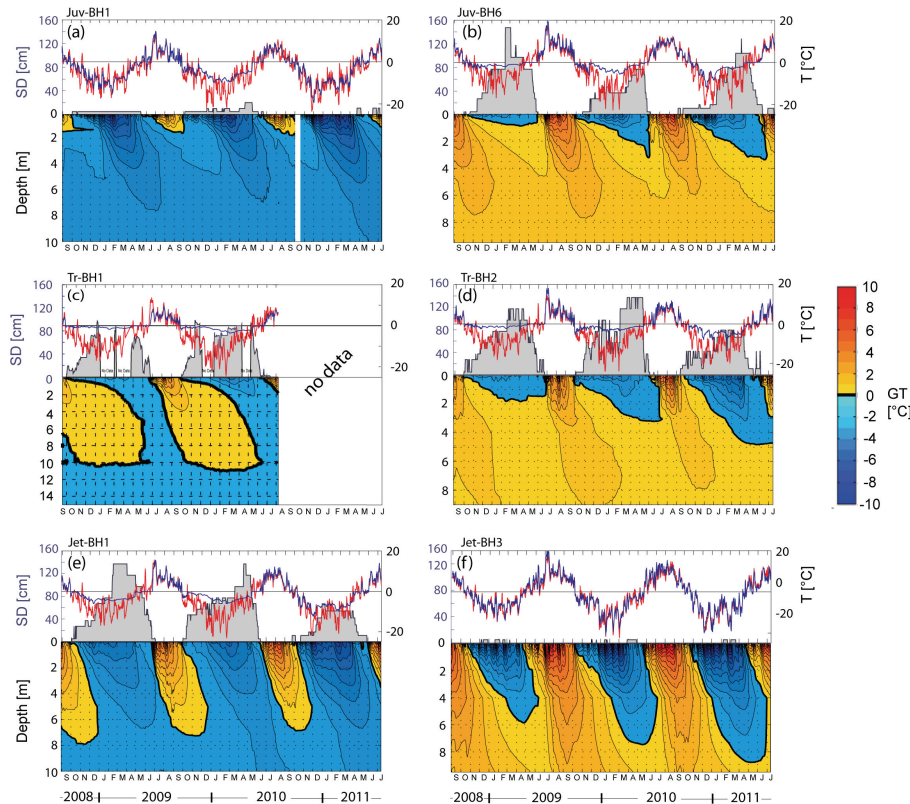
Fig. 3. Thermal regime of permafrost and non-permafrost borehole sites at Juvvasshøe **(a, b)**, Tron **(c, d)** and Jetta **(e, f)** comprising GT, GST, T_{AIR} and snow depth (SD). The upper panel in each figure shows T_{AIR} (red line), GST (blue line) and SD (grey area). The lower panel in each figure represents a depth-time diagram of GT.
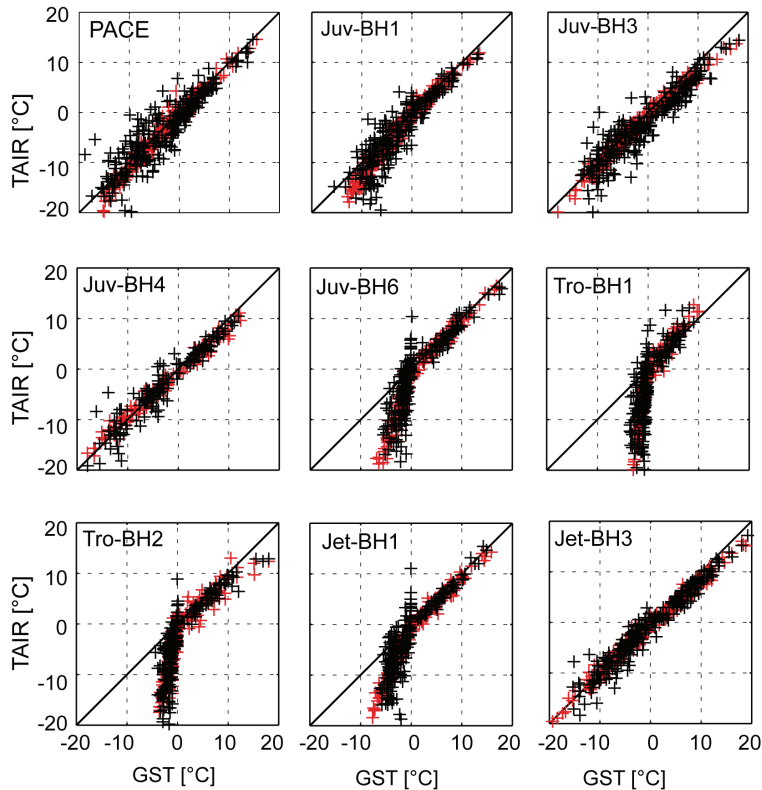
Fig. 4. Relationships between GST vs. T_{AIR} during the observation period 2008–2010 at the modelled boreholes. Black crosses: measured; red crosses: modelled. The snow-rich sites are clearly visible at the sharp kink at $T_{AIR} \sim 0\,°C$. The best correlations are found at sites with thin or no snow cover, (PACE , Juv-BH1 , Juv-BH3 to BH6). At sites with a long-lasting, thick snow cover (e.g. Tro-BH1, Jet-BH1), the *n*-factor-based GST model can still reproduce the GST pattern.

Title Page

Abstract | Introduction

Conclusions | References

Tables | Figures

◄ | ►

Back | Close

Full Screen / Esc

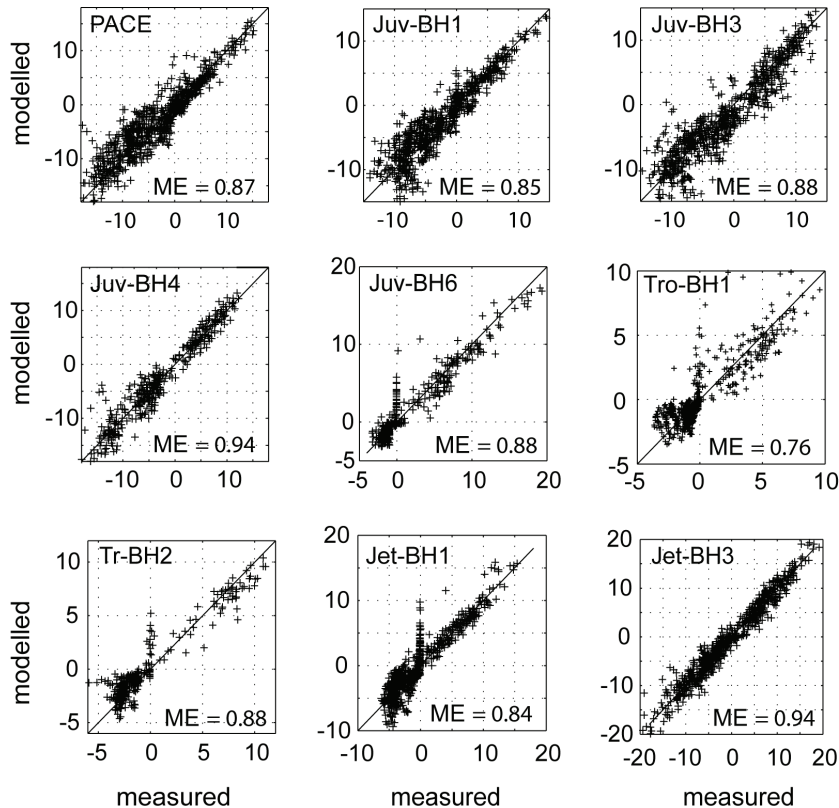Printer-friendly Version

Interactive Discussion

Fig. 5. Modelled vs. measured GST for the period 2008–2011 at modelled boreholes. In general, agreement between modelled and observed values is good with a Nash-Sutcliffe model efficiency coefficient ME > 0.80 (except for Tro-BH1). At bedrock sites and where the influence of snow cover was limited, an even better agreement was achieved (Juv-BH4, Jet-BH3) with ME > 0.90.

Title Page

Abstract | Introduction

Conclusions | References

Tables | Figures

◀ | ▶

◀ | ▶

Back | Close

Full Screen / Esc
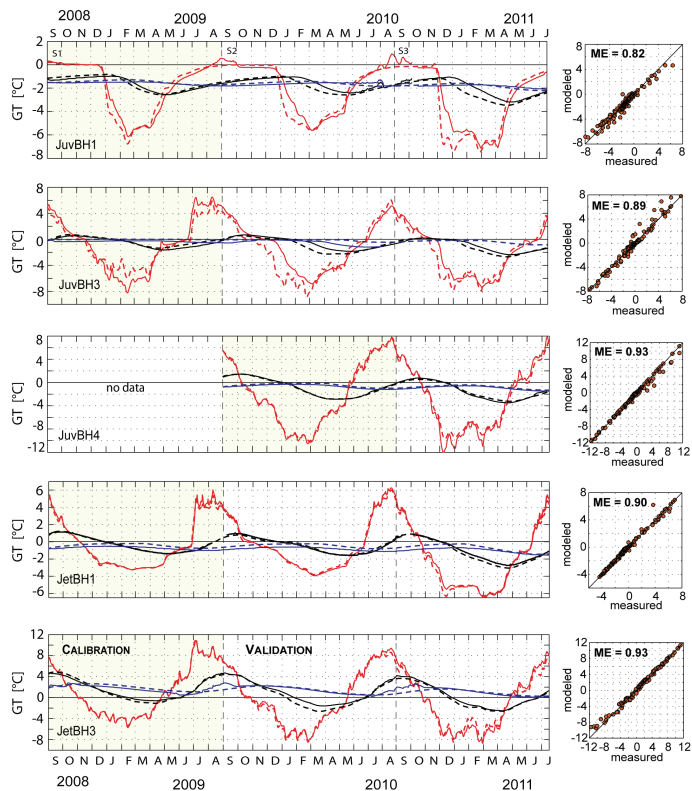
Printer-friendly Version

Interactive Discussion

Fig. 6. Left panels: Measured (solid lines) and modelled (dashed lines) ground temperatures (GT) at 1 m (red), 5 m (black) and 10 m (blue) depth during calibration (shaded area) and validation period. At Juv-BH4, data from S1 is not available and S2 served as calibration and S3 as validation period. Right panels: scatter plots showing measured against modelled GTs of validation period for all depths, including the depth-averaged Nash-Sutcliffe model efficiency coefficients (ME).

Title Page

Abstract | Introduction

Conclusions | References

Tables | Figures

|◄ | ►|

◄ | ►

Back | Close

Full Screen / Esc

Printer-friendly Version

Interactive Discussion

Discussion Paper | Discussion Paper | Discussion Paper | Discussion Paper
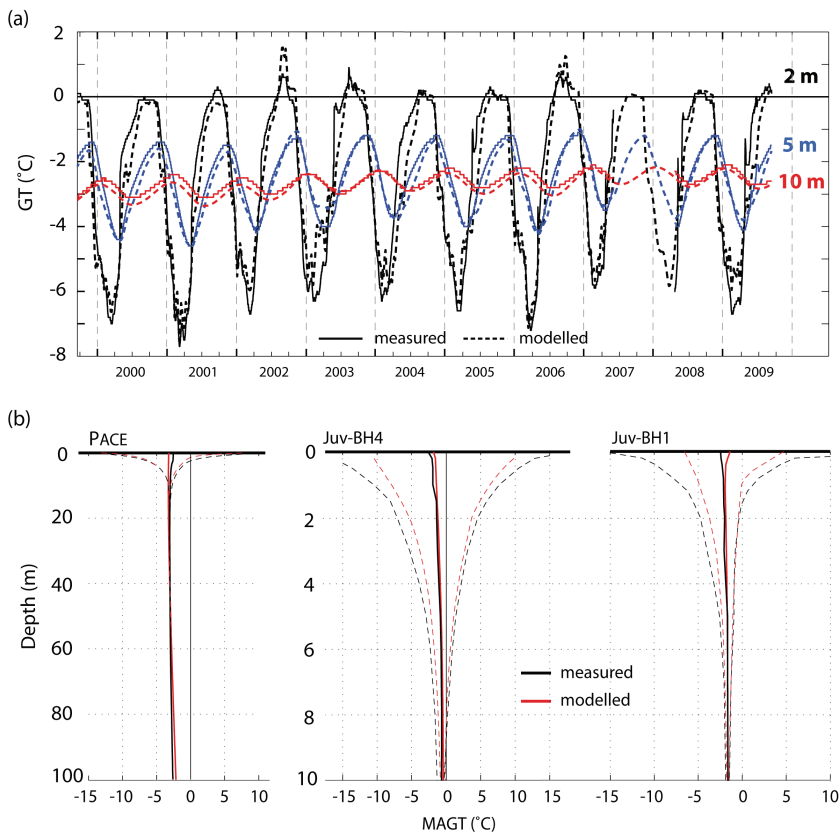
Fig. 7. Comparison of modelled to measured GTs during S1 after 150 model years. The model was run from steady state conditions for 1860 until 2008 using the reconstructed T_{AIR} series. Both, the seasonal dynamics during 1999–2008 at PACE **(a)** as well as the MAGTs **(b)** were reproduced with good accuracy (RMSE $< 0.7\,°C$) to a depth of 100 m (at PACE).

Discussion Paper | Discussion Paper | Discussion Paper | Discussion Paper |

TCD

6, 341–385, 2012

Modelling borehole temperatures in Southern Norway

T. Hipp et al.

Title Page

Abstract | Introduction

Conclusions | References

Tables | Figures

◀ | ▶

◀ | ▶

Back | Close

Full Screen / Esc

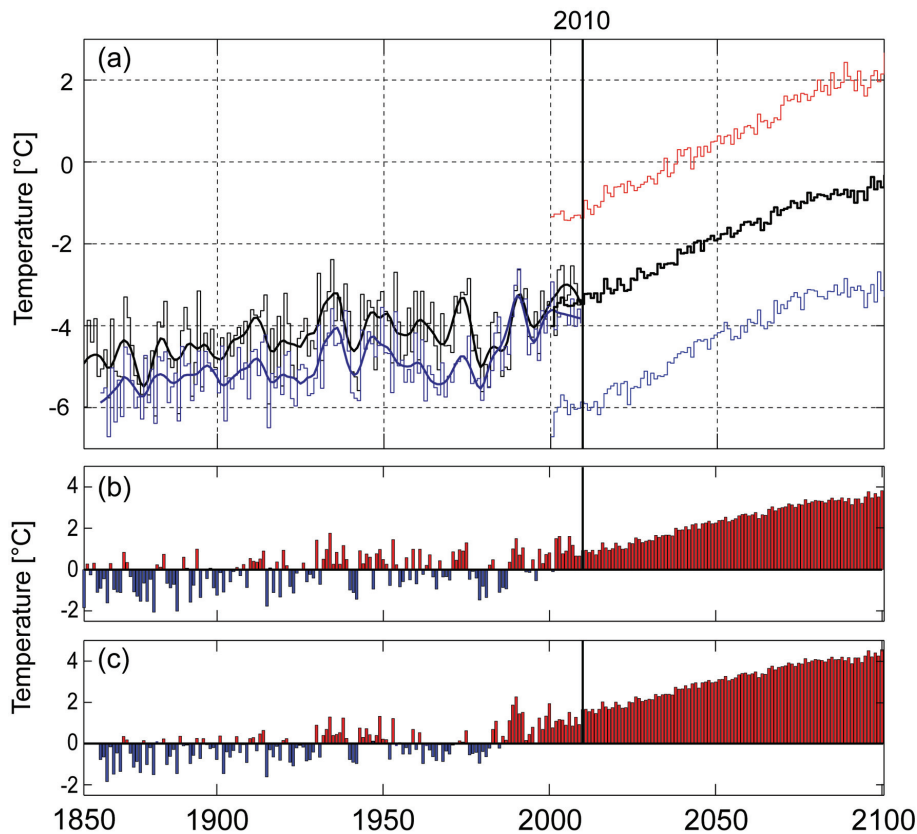Printer-friendly Version

Interactive Discussion

Fig. 8. (a) Historic air temperature series at the uppermost borehole at Juvvasshøe (black) and Tron (blue). The bold line represents the 7-yr Gaussian-filtered series. For 2010 onwards, the figure shows the median (bold black), 90 percentile (red) and 10 percentile (blue) of the downscaled T_{AIR} ensemble for Juv-BH1. The lower panels show the deviations of MAAT from the 1961–1990 climate normal at Juvvasshøe **(b)** and Tron **(c)**.
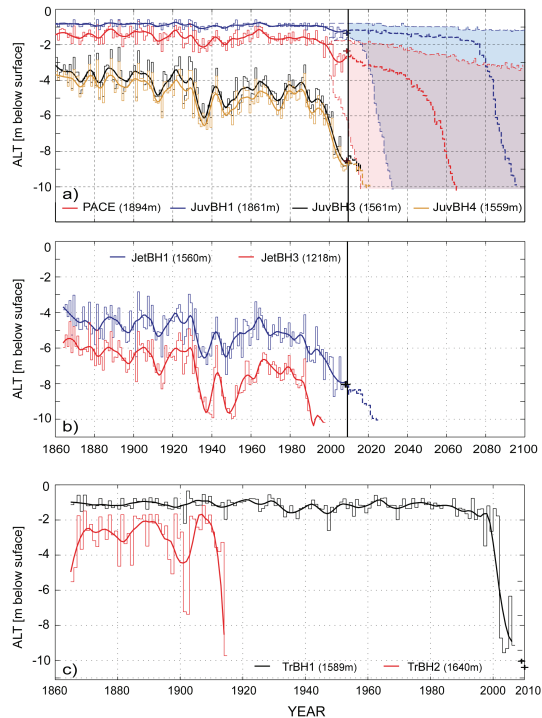
Title Page

Abstract | Introduction

Conclusions | References

Tables | Figures

|◄ | ►|

◄ | ►

Back | Close

Full Screen / Esc

Fig. 9. Reconstructed and projected active layer thickness (ALT) from 1860 to 2100 at Juvvasshøe **(a)**, Jetta **(b)** and Tron **(c)**. Projected ALT was modelled using the ensemble-median T_{AIR} (bold dashed lines). ForJuv-BH1 and PACE, also shown are ALT according to the 90 and 10 percentiles (shading) of the T_{AIR} ensemble. **(a)**. The bold lines represent a 7-yr Gaussian-filtered series, measured ALT are marked by crosses. The model indicates the permafrost degradation at Tron by the year 2010. Therefore, no projection was applied for Tr-BH1.
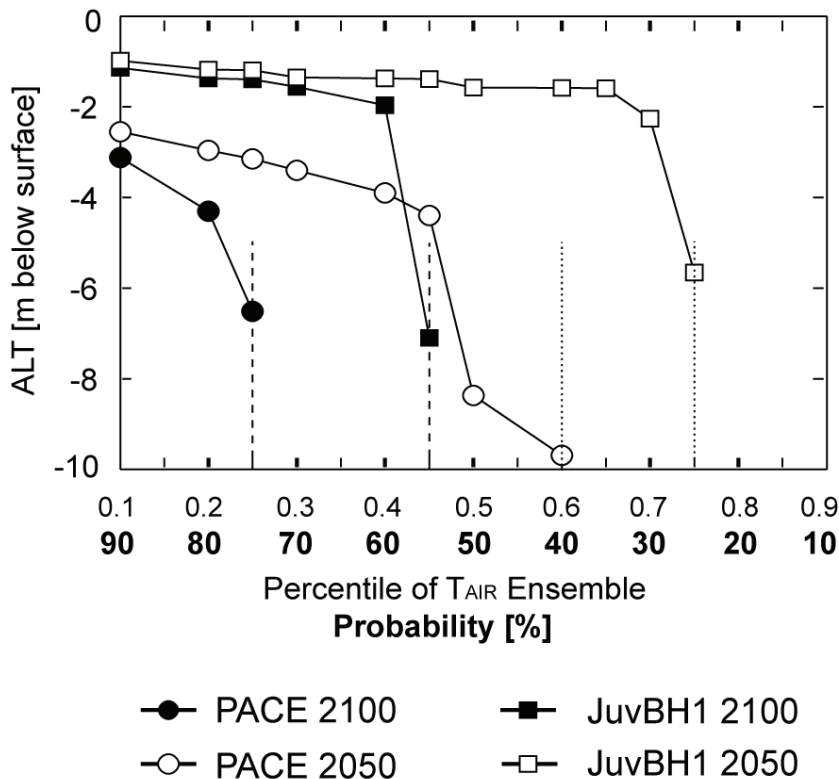
Fig. 10. Probability of permafrost degradation (no refreezing of the active layer) until 2050 (black) and 2100 (white) at Juv-BH1 (squares) and PACE (circles). The assessment is derived from model results for all percentiles of the T_{AIR} ensemble (in steps of 5%) and the probability is defined as the percentile at which seasonal refreezing of the active layer does not occurr anymore. Vertical lines mark the probability of this event occurring by 2050 (dashed) and 2100 (dotted), respectively.